Biophysical Journal
Article

Biophysical Society

Computational Study of Thrombus Formation and Clotting Factor Effects under Venous Flow Conditions

Vijay Govindarajan,[1] Vineet Rakesh,[1] Jaques Reifman,[1,*] and Alexander Y. Mitrophanov[1]
[1]Department of Defense Biotechnology High Performance Computing Software Applications Institute, Telemedicine and Advanced Technology Research Center, U.S. Army Medical Research and Materiel Command, Fort Detrick, Maryland

ABSTRACT A comprehensive understanding of thrombus formation as a physicochemical process that has evolved to protect the integrity of the human vasculature is critical to our ability to predict and control pathological states caused by a malfunctioning blood coagulation system. Despite numerous investigations, the spatial and temporal details of thrombus growth as a multicomponent process are not fully understood. Here, we used computational modeling to investigate the temporal changes in the spatial distributions of the key enzymatic (i.e., thrombin) and structural (i.e., platelets and fibrin) components within a growing thrombus. Moreover, we investigated the interplay between clot structure and its mechanical properties, such as hydraulic resistance to flow. Our model relied on the coupling of computational fluid dynamics and biochemical kinetics, and was validated using flow-chamber data from a previous experimental study. The model allowed us to identify the distinct patterns characterizing the spatial distributions of thrombin, platelets, and fibrin accumulating within a thrombus. Our modeling results suggested that under the simulated conditions, thrombin kinetics was determined predominantly by prothrombinase. Furthermore, our simulations showed that thrombus resistance imparted by fibrin was ~30-fold higher than that imparted by platelets. Yet, thrombus-mediated bloodflow occlusion was driven primarily by the platelet deposition process, because the height of the platelet accumulation domain was approximately twice that of the fibrin accumulation domain. Fibrinogen supplementation in normal blood resulted in a nonlinear increase in thrombus resistance, and for a supplemented fibrinogen level of 48%, the thrombus resistance increased by ~2.7-fold. Finally, our model predicted that restoring the normal levels of clotting factors II, IX, and X while simultaneously restoring fibrinogen (to 88% of its normal level) in diluted blood can restore fibrin generation to ~78% of its normal level and hence improve clot formation under dilution.

INTRODUCTION

The blood coagulation system is the first line of the human body's defense against vascular injuries (1–4). When a blood vessel is breached, a complex array of molecular and cellular reactions leads to the formation of a thrombus—a spatial structure consisting mainly of small blood cells (platelets) and the fibrous protein fibrin, which covers the site of injury and stops the hemorrhage (i.e., effects hemostasis). However, this normal hemostatic response may be insufficient in the case of severe injuries, when the naturally forming hemostatic thrombi do not possess sufficient mechanical resistance to stop the bleeding from large blood vessels. Moreover, severe trauma may lead to pathological changes (collectively known as trauma-induced coagulopathy (5)) that decrease the blood clotting potential in the trauma victim. Sometimes, genetic defects (e.g., hemophilia (2)) may decrease the clotting potential. Furthermore, pathological thrombi can form inside intact blood vessels, thereby occluding the blood flow in otherwise healthy tissues (i.e., causing thrombosis (4,6)). To predict and prevent such pathological conditions, or to reverse them using therapeutic interventions, a detailed mechanistic understanding of the thrombus formation process is needed.

Platelets and fibrin are the main structural components of a hemostatic thrombus (1,2,4,7,8). Fibrin is produced when its precursor, fibrinogen, is cleaved by the enzyme thrombin, which in turn is generated in a complex sequence of biochemical reactions when thrombus formation is initiated. The role of fibrin is to increase the mechanical stability of the growing thrombus by "tying together" the aggregated

Submitted January 21, 2015, and accepted for publication March 8, 2016.

*Correspondence: jaques.reifman.civ@mail.mil

Vineet Rakesh's present address is W. L. Gore & Associates, Inc., Newark, Delaware.

Editor: Fazoil Ataullakhanov.

http://dx.doi.org/10.1016/j.bpj.2016.03.010

platelets (and, if present, red blood cells) at the site of thrombus formation (4,8,9). The critical role of fibrin in vivo is illustrated by clinical cases involving patients with an inherited fibrinogen deficiency, who are prone to bleeding and need fibrinogen supplementation (10). Moreover, fibrinogen deficiency can occur as a result of trauma, and the use of fibrinogen blood supplements in trauma has been the subject of recent investigations (5). Fibrinogen supplementation during surgery has been shown to reduce postoperative bleeding (11). At the same time, elevated fibrinogen levels may contribute to the development of thrombosis (4,6,12). Quantitative knowledge about the interactions between fibrin and other clot components may allow us to achieve the desired balance in fibrinogen- and fibrin-mediated modulation of blood coagulation.

Fibrin biochemistry, structural biology, and rheology have been extensively investigated. Such studies provide information about the biochemical reactions leading to fibrin formation and polymerization, constituting molecular "parts" and three-dimensional shapes of fibrin fibers, as well as information about the physical properties of fibrin, such as its viscoelasticity (4,8,9,13,14). However, the details of fibrin accumulation as a spatiotemporal process remain elusive, and this lack of knowledge limits our understanding of the thrombus as a spatial structure whose composition may vary with time. Specifically, it is not clear how the spatial distribution of deposited platelets, thrombin, and fibrin can change in the course of thrombus development. More research is needed to understand the relative contributions of platelets and fibrin to the growing hydraulic resistance of the thrombus, and to the corresponding changes in blood flow. Finally, it is not known how the spatial distribution of fibrin in the clot, and the fibrin-associated mechanical properties of the clot, are modified in response to changes in the overall availability of fibrinogen and fibrin in the system. Here, we attempted to provide insights into these fundamental questions.

Blood coagulation has traditionally been studied using three approaches: in vitro experiments, in vivo experiments, and clinical investigations. Although these approaches provide valuable information about the blood-clotting process, each has its limitations. The recent emergence of systems biology has suggested a way to circumvent some of the limitations of traditional experimentation by combining experimental studies with the use of mathematical models (15,16). Such models can be designed to represent the mechanisms of the human blood coagulation process in realistic blood-flow conditions and vessel geometries, and can provide a flexible means to rapidly investigate a wide range of plausible thrombus formation scenarios. As such, these models can be practically useful when they are applied to predict drug targets and the effects of pharmacological intervention as a function of intervention time and drug dosage. Here, we use a computational systems biology approach to investigate fibrin accumulation as a spatiotemporal process during thrombus development in flowing blood.

The existing literature contains numerous examples of computational modeling of some aspects of blood coagulation under flow (15–30). However, previous modeling efforts did not focus on the investigation of relative contributions of platelets and fibrin to spatial thrombus growth. We developed and applied a model of thrombus formation under flow that captured the interplay of platelet deposition, complex thrombin-generation biochemistry, and fibrin formation and function, and was able to predict essential dynamic features of the thrombus formation process observed in flow-chamber experiments (31–33). Using the model, we elucidated the distinct spatial distributions of platelets, thrombin, and fibrin within the thrombus. Moreover, the model predicted that the occlusion of a flow-chamber channel by a growing thrombus is primarily driven by platelet deposition. Furthermore, in our modeling studies, we established that fibrinogen supplementation affects thrombus properties in a nonlinear fashion in the cases of both normal blood composition and diluted blood, which represents the conditions of dilution/consumption-induced coagulopathy that occur during trauma and surgery. Finally, the model predicted that supplementation with fibrinogen and with a prothrombin complex concentrate (PCC) can potentially improve the fibrin generation and accumulation kinetics in diluted blood, thereby improving clot formation.

MATERIALS AND METHODS

We developed a computational model that represents thrombus formation in a straight channel; this model was used in all the simulations described in this work. The model was implemented using the computational fluid dynamics package FLUENT v. 14.5 (ANSYS, Canonsburg, PA). Below is a description of the key model features; additional details, such as a full set of the model equations and a definition of our variable (i.e., shear-dependent) platelet adhesion rate constant, are provided in the Supporting Material. All of the model's parameter values were taken from literature data except for the maximal platelet density and platelet adhesion rate constant. The latter two parameters were fine-tuned to improve our model's quantitative accuracy with respect to the analyzed platelet deposition data, as described in the Supporting Material.

Model of the thrombus formation mechanism: platelet deposition and the biochemical coagulation network

The formation of a thrombus inside a blood vessel is manifested through the deposition and activation of platelets at the site of vascular injury and through thrombin-catalyzed fibrin generation. These complex processes are concurrent and interdependent, with the biochemical thrombin generation and fibrin formation network comprising dozens of intermediate biochemical species and reactions (Fig. 1). Our platelet activation model and the biochemical network model are modified versions of those developed by Leiderman and Fogelson (22). The Supporting Material includes a complete description of the platelet dynamics and biochemical reactions, together with the initial conditions and values of the kinetic constants (Eqs. S1–S55 and Tables S1–S8). In what follows, we provide a summarized description of the system.

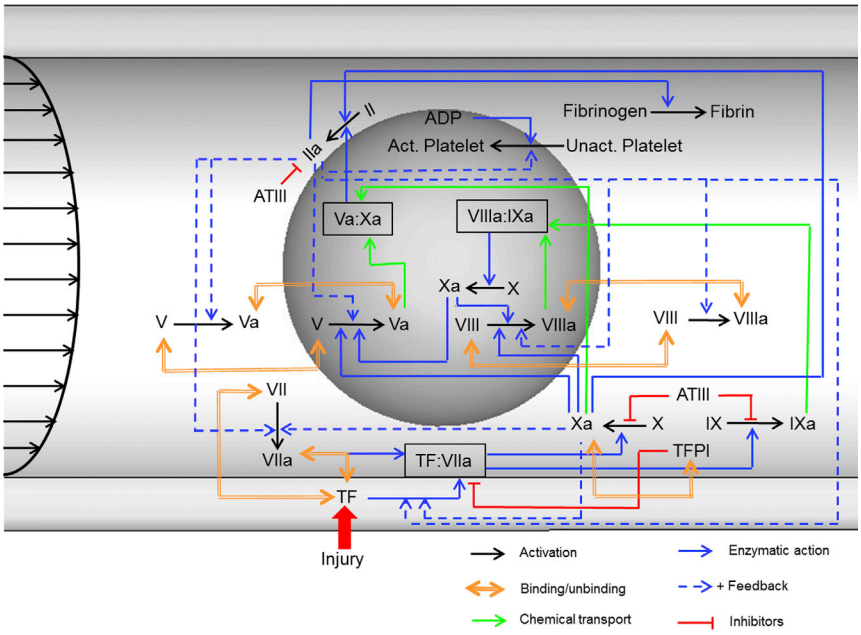

FIGURE 1 Schematic of the biochemical network represented in our model of blood coagulation. Coagulation reactions begin when blood leaking from a breached vessel comes into contact with the tissue factor (TF) expressed extravascularly. Colored arrows show the type of reaction, as indicated in the legend. Reactions shown inside the gray sphere are the platelet-surface reactions, and reactions outside the gray sphere are the reactions taking place in the blood plasma. The biochemical blood coagulation network comprises zymogens, proteolytic enzymes, and their cofactors. Among the key proteins (in an inactive form) are the factors V, VII, VIII, IX, X, and II (prothrombin). Their active counterparts are designated with the suffix "a." Reactions begin when TF is exposed to the flowing blood and binds with factor VIIa to form the TF:VIIa complex (extrinsic tenase). This is followed by the activation of factors IX and X to IXa and Xa, respectively, by TF:VIIa. Factor Xa in plasma activates plasma prothrombin to form trace amounts of factor IIa (thrombin). Platelet-bound factor Xa activates factors V and VIII to form factors Va and VIIIa, respectively. Factor IXa binds with factor VIIIa on the activated platelet surface to form the complex IXa:VIIIa (intrinsic tenase). Factor Xa binds with factor Va on the surfaces of activated platelets to form the complex Xa:Va (prothrombinase). Extrinsic and intrinsic tenases activate factor X to Xa, with intrinsic tenase acting as the main activator. Prothrombinase activates platelet-bound prothrombin to thrombin, which in turn performs several functions essential for efficient blood coagulation. Thrombin activates factors V and VIII, both on the surface of activated platelets and in plasma. This promotes the formation of intrinsic tenase and prothrombinase, acting as a positive feedback loop increasing thrombin generation. Importantly, thrombin converts fibrinogen to fibrin, which stabilizes the thrombus. The natural anticoagulation mechanisms (i.e., the TF pathway inhibitor and antithrombin III) negatively regulate thrombin generation and activity. The inhibitory protein antithrombin III (ATIII) inactivates several enzymes in the coagulation system, namely, factors IIa, Xa, and IXa, whereas the TF pathway inhibitor (TFPI) inhibits the TF:VIIa complex. To see this figure in color, go online.

Thrombus formation begins when platelets bind to collagen exposed at the site of vascular injury. Such binding leads to platelet activation, as a result of which platelet membranes acquire the ability to provide catalytic support for the biochemical reactions that lead to thrombin formation (Fig. 1). Thrombin itself is a potent platelet activator, which is reflected in our model. Platelets undergo transformations and interactions with each other that are governed by their evolution equations (Eqs. S1–S5). Briefly, when there are no external stimuli, platelets remain mobile and inactive (i.e., in the "resting" state). The mobile platelet types can convect, as determined by the fluid velocity field, and diffuse through the flow. Activated platelets can either stay mobile (i.e., able to convect and diffuse) or can bind with other bound and activated platelets or with the collagen exposed at the injury site (or at a thrombogenic surface), thereby becoming immobile. Activated platelets have the ability to accelerate the biochemical reactions (Fig. 1) occurring on their surfaces, and these biochemical reactions ultimately lead to thrombin generation.

The major differences between the biochemical network model used in this work and that in the original Leiderman-Fogelson (LF) model (22) are as follows. First, we have included a representation of the conversion of fibrinogen to fibrin (34) and a model for the impact of fibrin on thrombus formation. Representation of fibrin, which reinforces the mechanical bonds between platelets, is important, because it is generally considered essential for thrombus stability (4,8,31). Second, we have incorporated protein-specific binding-site numbers for zymogens and enzymes binding to platelet surfaces, with prothrombin and factor X sharing the binding sites (the details are provided in the Supporting Material). Third, we have included the activation of prothrombin to thrombin by the action of factor Xa in plasma (35). Finally, we omitted explicit representation of some intermediate enzyme-substrate complexes reflected in the LF model, which resulted in a reduction in the total number of model equations. This simplification assumes that the intermediate complexes are sufficiently short-lived; however, we explicitly represented all initial substrates and final products of the overall reaction, which are expected to perform a biological function of interest. It is consistent with the modeling approach in the biochemically rigorous and widely used Hockin-Mann model of thrombin generation (36). It has been recommended that simplified biochemical models should be used in conjunction with computational fluid dynamics flow modeling, especially when geometries for large blood vessels (e.g., coronary arteries) are involved (37). These considerations reinforced our decision to simplify the biochemical reactions in our model, because it was our intention to develop a model that allows for future extensions to perform full three-dimensional (3D) simulations for realistic, subject-specific vessel geometries.

Transport of platelets and coagulation proteins

The spatiotemporal kinetics of the biochemical species included in the model are governed by the convection-diffusion-reaction equation. The general form of this equation for a given species i is

$$\frac{\partial [C_i]}{\partial t} = -\nabla \cdot (\vec{u}[C_i]) + \nabla \cdot (D_i \nabla [C_i]) + R_i, \qquad (1)$$

where $[C_i]$ denotes the concentration of species i, $\vec{u}$ denotes the fluid velocity vector (each biochemical species has the same velocity as its surrounding fluid), and D_i represents the individual species diffusivity. We implemented interactions, such as platelet and protein activation and protein depletion, using the source term R_i and chose a second-order upwind scheme to discretize the convection-diffusion-reaction equation (38) with a convergence criterion of 10^{-6}.

In a tube-like flow chamber or a blood vessel, red blood cells have a tendency to aggregate in the center, thus forming a core (39). In addition, the biconcave-shaped red blood cells exhibit a tank-treading and tumbling

motion depending on the fluid viscosity, membrane elasticity, and the shear rate (40). This increases the effective diffusivity of the platelets and the plasma proteins. Hence, the diffusivity term in Eq. 1 should account for both the Brownian motion in blood plasma and the effect of red blood cells. To this end, we implemented the enhanced diffusivity model proposed by Zydney and Colton (41):

$$D_i^{\mathrm{e}} = D_i^{\mathrm{b}} + k d_{\mathrm{rbc}}^2 \varphi (1-\varphi)^{\eta} \dot{\gamma}, \tag{2}$$

where D_i^{e} and D_i^{b} denote the enhanced diffusivity and Brownian diffusivity, respectively, of species i, k and η represent empirical constants, d_{rbc} denotes the red-blood-cell diameter, φ represents the local hematocrit, which varies along the height of the flow-chamber channel, and $\dot{\gamma}$ denotes the local shear rate. We used the following definition for φ (the so-called "blunt" hematocrit profile, which gives an improved agreement with experimental data in comparison to other profiles (42)):

$$\varphi = \frac{\varphi_{\mathrm{b}}}{2}\left(1 - \cos\frac{\pi y}{\delta}\right), \tag{3}$$

where φ_{b} denotes the bulk hematocrit, y denotes the distance from the channel wall, and δ represents the thickness of the cell-free layer. We chose the latter to be 10% of the channel height, so that the hematocrit profile defined by Eq. 3 matched that of Hund and Antaki (42).

Besides enhancing diffusivity, the motion of red blood cells results in a nonuniform platelet distribution, with platelets tending to move toward the periphery of the blood flow. This effect is commonly called platelet margination and results in an increased platelet concentration near the wall (43–46). Platelet margination can be modeled by combining the expression for diffusivity with a potential function in the platelet-transport-governing equation (Eq. S1). The lateral drift of the platelets is then directed by the gradients of this potential (43,45,47). This takes into account the effect of the local hematocrit level on platelet margination (42,43,45,47). Models based on other simulation techniques, such as a combination of a master equation model of suspension dynamics and hydrodynamic Monte Carlo (48,49), explicit representation of red blood cells using a fixed red-blood-cell distribution (46), and deformable red blood cells based on the lattice-Boltzmann-immersed-boundary method (44), have also been developed to study platelet margination.

To capture platelet margination effects in our study, we implemented the platelet margination model developed by Bark and Ku (43) (see Eqs. 4 and 5 below). We chose this particular model because it showed that when used together with the enhanced diffusivity model from (41), this platelet margination model accurately captured the experimentally observed platelet flux for shear rates $<6000\ \mathrm{s}^{-1}$ (43). Moreover, this platelet margination model is naturally compatible with, and could be directly integrated in, our overall modeling framework. The equations describing the platelet flux are

$$\vec{N}_{\mathrm{p}} = \vec{u} C_{\mathrm{p}} - D_{\mathrm{p}}^{\mathrm{e}} \nabla \psi_{\mathrm{p}}, \tag{4}$$

$$\nabla \psi_{\mathrm{p}} = C_{\mathrm{p}} \nabla(\varphi) + \varphi \nabla\left(C_{\mathrm{p}}\right), \tag{5}$$

where $\vec{N}_{\mathrm{p}}$ denotes the platelet flux, C_{p} denotes the platelet concentration, $D_{\mathrm{p}}^{\mathrm{e}}$ represents the enhanced diffusivity introduced in Eq. 2, and ψ_{p} represents the platelet field potential, which is defined as a function of the local hematocrit level, φ (with a blunt inlet concentration profile, as described in Eq. 3, which is similar to the one used in (42) and (43)). The term $C_{\mathrm{p}}\nabla(\varphi)$ serves as the drift function, which enables platelets to move down the red-blood-cell gradient in the direction that is a function of the platelet concentration. The enhanced diffusivity determines the platelet transport rate, whereas the potential in Eqs. 4 and 5 drives platelets in a specific direction based on the gradients of red blood cells and platelets in the flow (43).

Modeling the effect of a growing thrombus on blood flow

Blood flow in our model is governed by the incompressible Navier-Stokes equation. The effect of a thrombus on the blood flow is represented via a reduction of fluid velocity in the region occupied by the growing thrombus, as detailed below. The thrombus is represented by a growing porous medium whose permeability depends on the increasing fractions of deposited platelets and the fibrin concentration. This is achieved by incorporating additional source terms into the Navier-Stokes equation, as follows:

$$\nabla \cdot (\vec{u}) = 0; \tag{6}$$

$$\rho\left(\frac{\partial \vec{u}}{\partial t} + (\vec{u} \cdot \nabla)\vec{u}\right) = -\nabla p + \mu \Delta \vec{u} - \frac{\mu}{K_{\mathrm{t}}(x)}\vec{u}, \tag{7}$$

where $\vec{u}$ denotes the fluid velocity vector, ρ represents the blood density, p represents the fluid pressure, μ denotes the dynamic viscosity of blood, and the term $\mu/K_{\mathrm{t}}(x)$ in Eq. 7 is known as the Brinkman term, where $K_{\mathrm{t}}(x)$, which depends on the space point x, represents the permeability of a porous medium and $1/K_{\mathrm{t}}(x)$ represents its hydraulic resistance (50).

To solve the Navier-Stokes equation (Eqs. 6 and 7), we employed the PISO (i.e., pressure implicit with splitting of operators) algorithm available in FLUENT to couple the velocity and the pressure. We chose PISO over other schemes because, in addition to producing stable results, it allows the use of large time steps in unsteady flow problems (51). The second-order upwind scheme is used for the spatial discretization of the momentum equation (Eq. 7). The pressure interpolation was performed using the "pressure staggering" option (PRESTO!) (52). The PRESTO scheme uses the discrete continuity balance for the staggered control volume to compute the pressure. This procedure, implemented in FLUENT, is similar to the staggered-grid scheme used with structured meshes (52,53). Numerical convergence was achieved by setting a convergence criterion of 10^{-6} for continuity and velocity, and the solution was iterated until convergence of each time step. We used the algebraic multigrid method (AMG) with BCGSTAB (i.e., the biconjugate gradient stabilized method) stabilization available in FLUENT to achieve a faster and smoother convergence during the iterative procedure (54). Under-relaxation factors of 0.3, 0.7, and 1.0 were used for pressure, momentum, and the concentrations of all biochemical species, respectively.

In our model, the hydraulic resistance is imparted by the deposited platelets and fibrin. The individual contributions of hydraulic resistances from platelets and fibrin are added (55,56), and $1/K_{\mathrm{t}}$ in Eq. 7 is expressed as

$$\frac{1}{K_{\mathrm{t}}} = \frac{1}{K_{\mathrm{p}}} + \frac{1}{K_{\mathrm{f}}}, \tag{8}$$

where K_{p} and K_{f} are the permeability of platelet and fibrin mass, respectively.

We computed the contribution of the platelets to the total hydraulic resistance as (22)

$$\frac{1}{K_{\mathrm{p}}} = \alpha_{\max}\left(\frac{(\varphi^{\mathrm{b}})^2}{\left(\varphi_o^{\mathrm{b}}\right)^2 + (\varphi^{\mathrm{b}})^2}\right), \tag{9}$$

where φ^{b} denotes the fraction of bound platelets, which is the ratio of bound platelets to the maximal possible platelet density, and φ_0^{b} is a constant; when $\varphi^{\mathrm{b}} = \varphi_0^{\mathrm{b}}$, the frictional resistance reaches half of its maximal value. Leiderman and Fogelson (22) estimated $\alpha_{\max}$ (inverse permeability) to be sixfold larger than the values observed in old thrombi extracted from abdominal aortic aneurysms, which had a permeability value of $0.91 \pm 0.54\ \mathrm{mm}^4\ \mathrm{N}^{-1}\ \mathrm{s}^{-1}$ (57).

In the thrombus, fibrin is naturally present in a polymeric state, which reduces its mobility under flow (58). Because fibrin polymerization is not explicitly represented in our model, we accounted for fibrin's reduced mobility by assuming that it cannot convect with the flow. It should be noted that although fibrin can diffuse in the domain, its diffusion is comparatively slow; indeed, its diffusion coefficient is the lowest among all the modeled species (34) (Table S1). To predict the hydraulic resistance imparted by fibrin, we used the Davies equation (59), which has often been used to estimate the permeability of fibrin gels and blood clots (30,56,60–62):

$$\frac{1}{K_f} = \frac{16\varphi_f^{1.5}\left(1 + 56\varphi_f^3\right)}{a_f^2}, \tag{10}$$

where a_f denotes the fiber radius and φ_f denotes the ratio of the fibrin concentration to that of fibrinogen. Fibrin permeability values predicted using the Davies equation were in reasonable agreement with experimental measurements (56).

Modeling blood dilution and supplementation with fibrinogen and a prothombin complex concentrate

To represent blood dilution, we followed our previous work and used an unequal blood dilution model, in which different coagulation factors are diluted to different degrees (63). This model was based on an in vivo porcine model of dilution-induced coagulopathy (64). In our model, dilution was implemented by reducing the initial concentrations of coagulation proteins by the appropriate amounts (see Table S9); these amounts were derived from our previous work (63,65). The diluted concentration for fibrinogen was chosen to be 40% of the normal level, which is consistent with in vivo data (64). Note that platelets were not diluted, so as to reflect the compensatory platelet resupply (e.g., from the spleen into the bloodstream) expected to occur in vivo (63). To represent the supplementation with a PCC, which is a combination of procoagulant clotting factors aimed at enhancing thrombin generation, we restored the corresponding PCC components (i.e., coagulation factors FII, FIX, and FX used in a typical three-factor PCC (66)) to their undiluted levels (see Table S9), in accordance with our previous work (65).

Simulated flow conditions

We simulated thrombus formation in a channel of the eight-channel pressure-relief flow chamber described by Maloney et al. (67) and Colace et al. (31). Fig. 2 A shows a photograph of the flow chamber and the computational domain used in our thrombus formation simulations. Fig. 2 *B* shows the 3D geometry of the flow-chamber section consisting of two channels measuring 250 × 60 μm (base × height) at their cross section. In the two-dimensional (2D) representation of the flow chamber (Fig. 2 *C*), two channels, each measuring 60 μm in height, are stacked one above the other, which allows us to perform the "pressure relief" mode simulations in a 2D setting (31). Thrombus formation was initiated in one of the two channels, which contained a thrombogenic surface coated with tissue factor (TF) and collagen. Imaging of the thrombogenic patch led us to estimate the tissue factor surface coverage as 10 molecules/μm^2 (31).

The 2D flow domain analyzed in this study consisted of two separate inlets and a single outlet with corresponding boundary conditions (Fig. 2 *C*). We simulated the pressure-relief mode (introduced in (31)) by defining a constant-pressure (i.e., atmospheric pressure) boundary condition at the inlet and a constant flow rate of 4 μL/min at the outlet, which corresponds to an initial wall shear rate of 200 s^{-1}. Because Colace et al. (31) used whole blood in their flow-chamber experiments, we chose a hematocrit value of 0.4, a typical value for this parameter. These settings make our simulation consistent with their experimental conditions. The simulation covered a 430-s time interval with a 0.01-s time step. A no-slip and no-penetration condition was imposed at the flow-chamber walls. In our simulations, thrombus formation was initiated in one of the channels at a 250-μm-long thrombogenic strip (Fig. 2 *C*), with TF levels matching the experimental setup (31). The initial concentrations (Table S3) of the coagulation proteins were taken from the experimental literature and adjusted to represent whole-blood concentrations. To describe the expected, nonuniform distribution of platelets over the channel's cross section, we used the near-wall platelet concentration profile defined in Eckstein et al. (68) with a peak/center ratio of 8.00. We used this profile to define the inlet profile for

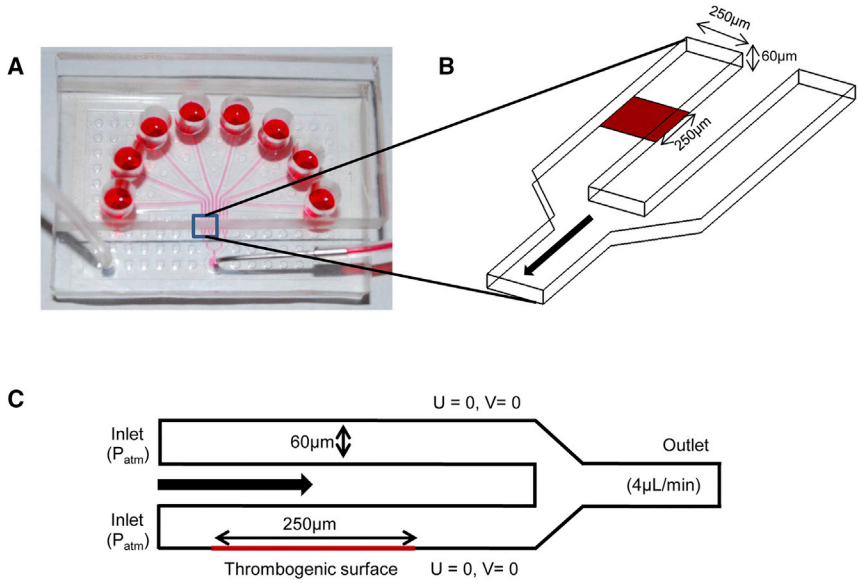

FIGURE 2 Two-dimensional (2D) geometric representation of the flow chamber. (*A*) Photograph of the overall setup of the flow chamber (image reproduced with permission from Colace et al. (31)). Thrombus formation is initiated when blood flows over a thrombogenic surface in the chamber's channels. Under the pressure-relief mode, one of the channels is coated with a thrombogenic surface. When a thrombus begins to occlude the channel, blood flow is increased in the thrombus-free channel to maintain a constant outflow (withdrawn from a syringe at the outlet) (31). (*B*) Three-dimensional geometry of the flow-chamber section that consists of two separate inlets and a single outlet. The dimensions of the channels are as indicated in the figure. (*C*) The geometry of the flow chamber was constructed to provide a 2D representation (as in (31)). This 2D geometry was constructed so that it maintained a channel height of 60 μm. The channel without a thrombogenic surface is stacked above the channel with one. This reconstructed geometry allowed us to perform simulations in the pressure-relief mode in a 2D setting. Also indicated are the flow boundary conditions used in our simulations. The notation U = 0, V = 0 reflects the no-slip and no-penetration conditions imposed on the walls, where U and V denote the x and y velocity components, respectively. To see this figure in color, go online.

inactive, mobile platelets. The computational domain was discretized with a uniform mesh size of 1.875 μm, which is adequate for resolving the species transport and flow (22).

RESULTS

Modeling predicts essential kinetic features of thrombus formation

The model-predicted time course of platelet deposition initiated by the thrombogenic surface was consistent with the platelet accumulation data presented in Colace et al. (31), which show an approximately linear time dependence (Fig. 3 *A*). As expected, activated and bound platelets continued to accumulate at the thrombogenic surface throughout the simulation, and the predicted height of the platelet deposition domain at 430 s was ~39 μm at the upstream and downstream sides of the thrombogenic surface and ~32 μm at the middle (Fig. 3 *B*, *bottom*). Interestingly, the simulated spatial distribution of the accumulated platelets extended beyond the upstream and downstream edges of the thrombogenic surface (Fig. 3 *B*), which is in accord with experimental observations (see Fig. 7 B in (31)). Fibrin was produced over the thrombogenic surface simultaneously with platelet deposition, and the predicted height for fibrin deposition reached ~16 μm at 430 s (Fig. 3 *C*). The spatial boundaries of the model-predicted platelet- and fibrin-deposition domains were in reasonable agreement with those determined experimentally (Fig. 3 *B*, *bottom*, and Fig. 3 *C*, respectively).

In our model, fibrin generation depends on thrombin generation, which dynamically changes during thrombus growth. During the initial 220 s of the simulation, very little thrombin (and, therefore, little fibrin) was generated in the flow chamber; this was followed by a sharp, nonlinear rise in the thrombin concentration (Fig. 4 *A*). This thrombin burst thus appeared to be responsible for generating the bulk of fibrin in the growing thrombus. Indeed, after an initial lag phase, our model showed a rapid nonlinear increase in fibrin production that followed the rise in thrombin generation (Fig. 4 *B*). Although the model-predicted platelet deposition kinetics and the spatial boundary of the thrombus (i.e., bound platelets and fibrin) compared reasonably well with the experiment of Colace et al. (31) (Fig. 3, *B* and *C*), our model did not capture the temporal dependence of fibrin accumulation from that work (see Fig. 4 *B*), which shows the normalized integral of the model-predicted fibrin concentration calculated over the entire flow domain). In contrast to our findings, that experimental work reported an approximately linear increase in fibrin deposition after a very small lag phase (Fig. 4 *B*). Yet the fibrin-deposition kinetics observed in other flow-chamber studies (32,33) qualitatively agreed with our results (Fig. 4 *B*). Indeed, both of these experimental studies (performed at different venous shear rates) reported a lag in fibrin production

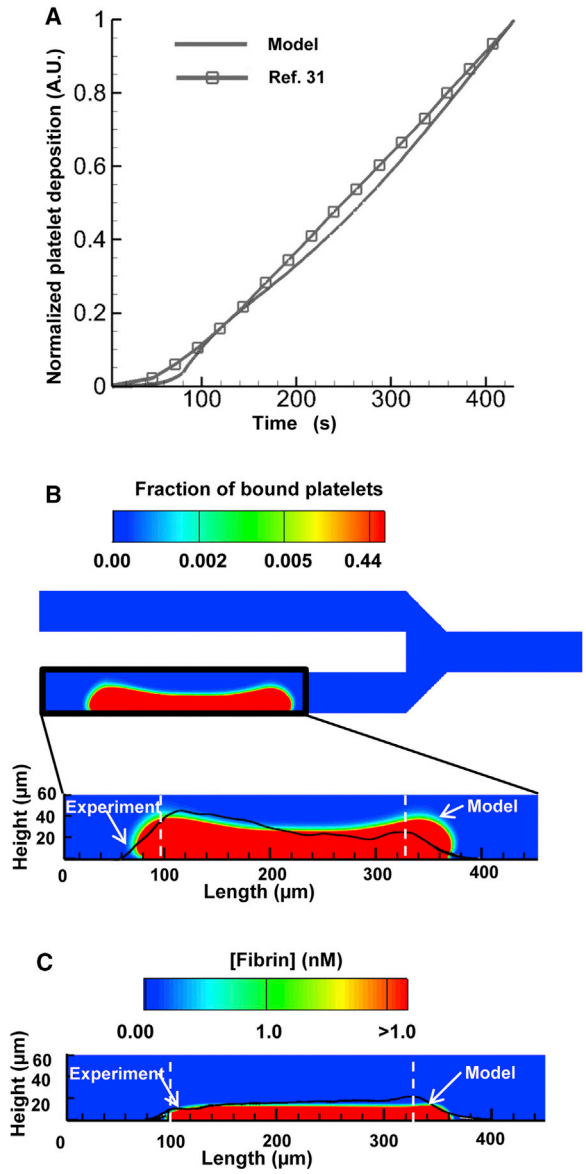

FIGURE 3 The computational model captures the dynamics of thrombus growth. (*A*) Model-predicted and experimentally measured platelet accumulation. The solid line (no symbols) shows the normalized model-predicted values of the integral of the concentrations of bound platelets calculated over the entire flow domain. The solid line with square markers shows normalized platelet fluorescence intensity, which represents platelet accumulation observed in the flow-chamber experiment (31). Data points, represented by the markers, were connected with solid lines to enhance the visual representation of the displayed trends. To facilitate data comparisons, the model-generated and experimental data were independently normalized to their corresponding maximal values. (*B*) Spatial distribution of the deposited platelets at 430 s. The bottom panel shows an enlargement of the model-predicted platelet deposition domain. The experimentally measured platelet accumulation (data extracted from Fig. 7 B in (31)) is indicated by the black line superimposed over the color image. The vertical white dashed lines indicate the beginning and end of the thrombogenic surface. (*C*) Spatial distribution of the deposited fibrin at 430 s. The experimentally measured fibrin accumulation (data extracted from Fig. 7 *C* in (31)) is indicated by the black line superimposed over the color image. The vertical white dashed lines indicate the beginning and end of the thrombogenic surface. To see this figure in color, go online.

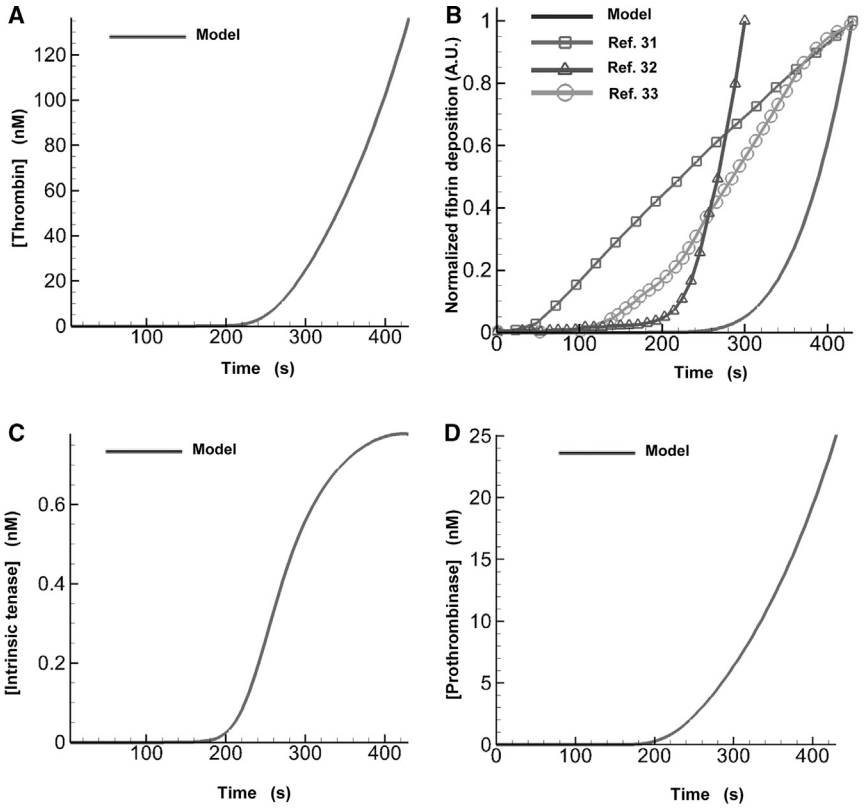

FIGURE 4 Fibrin deposition is determined by thrombin generation. (*A*) Time-dependent maximal values of the model-predicted spatial distribution of thrombin concentration. (*B*) Fibrin deposition predicted by the model is compared with data from flow-chamber experiments. The solid line (no symbols) shows the normalized integral of the model-predicted fibrin concentration calculated over the entire flow domain. The lines with markers represent the normalized fibrin levels (determined using fluorescence-intensity measurements) reported in different flow-chamber experiments. Data points, represented by the symbols, were connected with solid lines to enhance the visual representation of the displayed trends. To facilitate data comparisons, the model-generated and experimental data were independently normalized to their corresponding maximal values. (*C*) Time-dependent maximal values of the model-predicted spatial distribution of the intrinsic tenase concentration. (*D*) Time-dependent maximal values of the model-predicted spatial distribution of the prothrombinase concentration.

followed by a sharp, nonlinear rise in the fibrin level, as was predicted by our model. Taken together, these results indicate that some details of thrombus formation kinetics may differ depending on the experimental setup. Our model may not reproduce such nuances, but it appears to capture some of the main experimentally observed trends.

It is generally known that thrombin generation is strongly influenced by the activity of two main enzyme complexes, intrinsic tenase (VIIIa:IXa) and prothrombinase (Va:Xa), formed on platelet surfaces (36,69). To obtain insights into their roles in shaping thrombin kinetics under flow, we plotted their time courses (Fig. 4, *C* and *D*) and compared them with that of thrombin (Fig. 4 *A*). Interestingly, the prothrombinase kinetics were qualitatively similar to that of thrombin, whereas the intrinsic tenase kinetics were different. As could be expected, the prothrombinase kinetics slightly preceded the thrombin kinetics, reflecting the causal relationship between prothrombinase activity and thrombin generation. These results suggest that, under the conditions of our simulation, thrombin kinetics is determined primarily by prothrombinase rather than by intrinsic tenase.

Platelets, thrombin, and fibrin are characterized by distinct spatial distributions in the thrombus

Our model reflected the temporal process of platelet accumulation at the thrombogenic surface location (Fig. 5). As expected, initially there was no detectable platelet deposition (Fig. 5 *A*). During the first 100 s of the simulation, a thin layer of platelets was deposited at the thrombogenic surface (Fig. 5 *B*). By ~200 s, the platelet deposition had grown and was blocking ~27% of the flow-chamber height, with a higher fraction of platelets present near the thrombogenic surface (Fig. 5 *C*). These platelets were activated predominantly by collagen (~63%) and ADP (~32%), because substantial amounts of thrombin were seen only at times exceeding 220 s after thrombus formation initiation (Fig. 4 *A*). From 220 s onward, the sharp increase in thrombin level (Fig. 4 *A*) began contributing to the accumulation of activated platelets, thereby accelerating the clot's growth (Fig. 5, *C–E*). Throughout the process, platelets continued to accumulate, occluding the flow chamber (Fig. 5, *B–E*). At the end of the simulation (Fig. 5 *E*), platelets were blocking ~65% of the flow-chamber height.

In our simulation, thrombin and fibrin were more or less uniformly distributed over the thrombogenic surface, with a slight increase in concentration at the downstream side (Fig. 6), which qualitatively agrees with experimental observations (Fig. 7 C of Colace et al. (31)). At 100 s of the simulation, our model predicted sparse formations of thrombin spatially distributed on both the upstream and downstream sides of the thrombogenic surface (Fig. 6 *B*, *left*). This thrombin converted small amounts of fibrinogen to fibrin (Fig. 6 *B*, *right*). By 200 s, our model predicted a slight increase in thrombin (Fig. 6 *C*, *left*) and a resulting increase in fibrin (Fig. 6 *C*, *right*). Around 220 s after thrombus

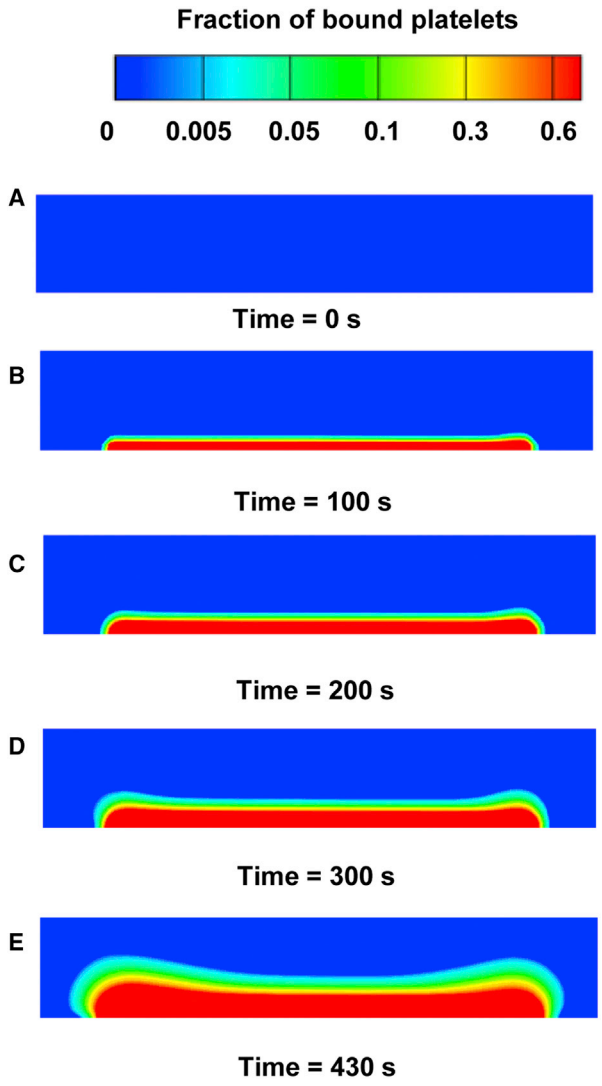

FIGURE 5 Spatial distribution of bound platelets deposited at the thrombogenic surface. (*A–E*) The colors represent the fraction of bound platelets at distinct times in the simulation. This fraction was calculated as the concentration of bound platelets divided by the maximal possible number of platelets in a unit volume (see Supporting Material for details). Only the flow-chamber channel with the thrombogenic surface is shown. To see this figure in color, go online.

formation initiation, the rate of thrombin and fibrin generation increased. Indeed, shortly after 220 s, the thrombin concentration had exceeded 1 nM and reached the sharp-rise phase (Fig. 4 *A*). Consequently, from 220 s onward, we expected, and witnessed, a dramatic increase in fibrin levels (Fig. 6, *D–E*, *right*).

Our simulation showed that the spatial distribution of fibrin was concentrated beneath the deposited platelets and did not extend beyond the distribution of the platelets at any time during the simulation. The hydraulic resistance imparted by 50 nM of fibrin (a concentration achieved within ~300 s in our simulation) exceeded that imparted by the deposited platelets at their maximal possible density (results not shown). This suggests that a concentration of 50 nM can be viewed as the threshold concentration beyond which fibrin strongly impacts the behavior of the thrombus by altering its resistance to blood flow. The additional resistance to the growing thrombus imparted by the increasing local fibrin concentration could further reduce the local blood-flow velocity inside the thrombus (Fig. S3), thereby decreasing the momentum imparted by the fluid to adjacent thrombus particles. This could effectively increase clot stability, which reflects the ability of the clot to resist the blood flow and to maintain structural integrity.

Occlusion of the flow chamber is dominated by platelet deposition

At the start of the simulation, blood freely moved through the flow chamber, because there were no accumulated platelets or fibrin (Fig. 7 *A*). Equal amounts of blood per unit time flowed through both channels (with and without a thrombogenic surface) of the chamber, converging at the outlet, where flow velocity was twofold higher than at the inlet, due to conservation of mass. As thrombus formation proceeded, regions of high resistance began to form, occluding the flow. Until 200 s after thrombus formation initiation (Fig. 7, *B* and *C*), resistance imparted to the flow was mostly due to platelet deposition, because there was no substantial accumulation of fibrin. Hence, hydraulic resistance due to platelet deposition appeared sufficient to alter the blood flow in the flow chamber. Throughout the simulation, the bottom channel experienced occlusion due to thrombus growth, and there was a corresponding increase in blood flow in the upper channel (Fig. 7, *B–E*).

The increased fibrin deposition over the thrombogenic surface (Fig. 6, *C–E*, *right*) correlated with the increased hydraulic resistance at the downstream side of the thrombus (Fig. 7, *D* and *E*, *left*). This suggests that increasing hydraulic resistance was more strongly driven by fibrin than by the accumulation of platelets, which showed a noticeably more uniform distribution along the thrombogenic surface (Fig. 5). In fact, the model-predicted maximal hydraulic resistance imparted by fibrin at the end of the simulation was up to ~30-fold higher than that imparted by platelets. (By comparison, Colace et al. observed that fibrin increased thrombus strength by up to 28-fold (31).) Nevertheless, the area of low axial velocity in the flow through the chamber (Fig. 7, *B–E*, *right*) mimicked the symmetric distribution of platelets in the thrombus, which extended beyond the area of fibrin accumulation (Fig. 5, *B–E*). Because decreased axial velocity is the main physical indicator of flow occlusion, this result demonstrates that flow-chamber occlusion was due mainly to platelet accumulation. This, in turn, implies that the hydraulic resistance of the upper portion of the thrombus (due largely to platelets) was sufficient to force the flow to bypass the thrombus area. Yet the increased hydraulic resistance and fibrin accumulation

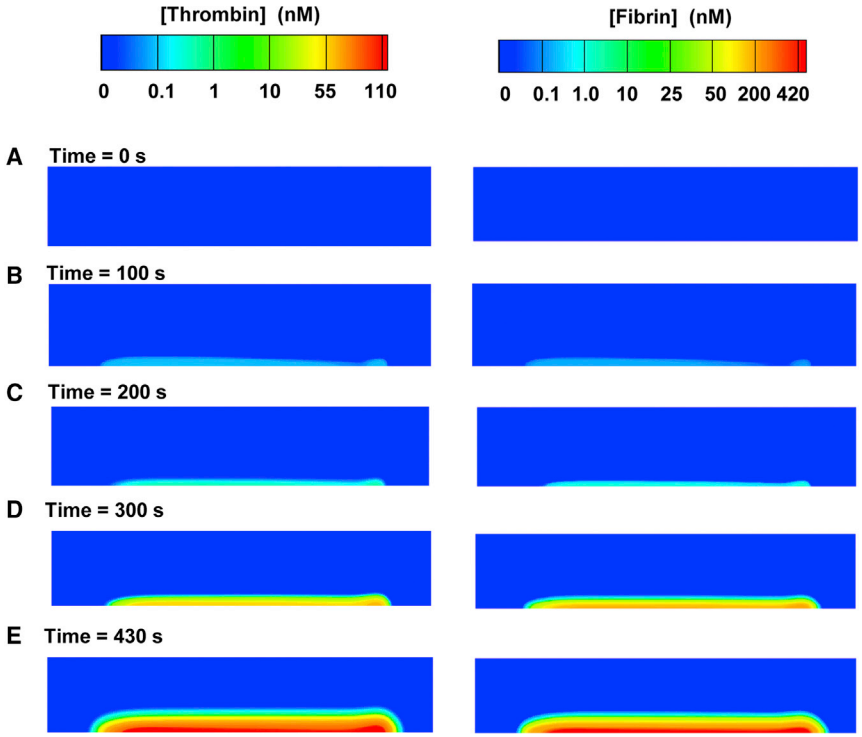

FIGURE 6 Spatial distribution of generated thrombin (*left*) and deposited fibrin (*right*) in the simulation. (*A–E*) The colors represent the concentrations of thrombin and fibrin at distinct times in the simulation. Only the flow-chamber channel with the thrombogenic surface is shown. To see this figure in color, go online.

suggest that the lower part of the thrombus would be more stable (as explained in the previous subsection) than its upper part.

Fibrinogen supplementation impacts the hydraulic resistance (clot strength) in a nonlinear fashion

To investigate the effect of fibrinogen supplementation on thrombus formation, we performed three additional simulations, increasing the fibrinogen level by 16%, 32%, and 48% of the default fibrinogen level (all other simulation conditions were kept constant; see Materials and Methods). Our model predicted that for all considered fibrinogen levels (i.e., 100%, 116%, 132%, and 148%), the fibrin concentration threshold of 50 nM (i.e., the threshold beyond which the hydraulic resistance (clot strength) imparted by fibrin exceeds that imparted by deposited platelets) was reached at ~300 s in the simulation (results not shown). This result illustrates that the onset time of the fibrin-generation surge did not strongly depend on the fibrinogen level. Yet, at the end of the simulations, we observed a notable difference in the maximal fibrin level between different fibrinogen supplementation scenarios (Fig. 8 *A*). This result indicates that during the later phases of thrombus formation, thrombus strength may depend significantly on the blood fibrinogen level.

In our simulations, we increased the fibrinogen level in a linear fashion. However, the corresponding increase in the maximal hydraulic resistance imparted by fibrin was strongly nonlinear (Fig. 8 *B*). The region of maximal resistance was located at the downstream side of the thrombogenic surface (~320 μm downstream from the inlet), where fibrin concentration was higher (indicated with a white line in Fig. 8 *C*). Moreover, although the increase in the fibrinogen level did not exceed 50%, the maximal hydraulic resistance increased by ~2.7-fold. By comparison, the fibrinogen-dependent increase in the fibrin level was smaller and did not exceed ~1.7-fold (Fig. 8 *A*). Therefore, the large fibrinogen-dependent change in hydraulic resistance was due primarily to the nonlinearity of the expression describing the fibrin level's effect on hydraulic resistance (Eq. 8).

Based on these results, we anticipated a fibrinogen-dependent increase in the hydraulic resistance in the area of fibrin accumulation within the thrombus, i.e., in its lower part adjacent to the thrombogenic surface. A comparison of the thrombus shape for 100% and 148% fibrinogen confirmed this expectation (Fig. 8 *C*, *red area*). Yet the overall area of heightened hydraulic resistance imparted by fibrin remained nearly unchanged (Fig. 8 *C*). This result suggests that fibrinogen supplementation did not impact the shape or size of the thrombus, resulting in an unchanged total flow profile (Fig. S1). This finding is consistent with our simulation for the default fibrinogen level, which suggested that the thrombus shape and size were determined primarily by platelet deposition rather than by fibrin accumulation (Figs. 5 and 7). Interestingly, a recent modeling study, which used a model with explicit representation of platelets as mechanical particles, suggested that initial fibrinogen concentration can impact the number of deposited platelets and, therefore, clot size (70). These results

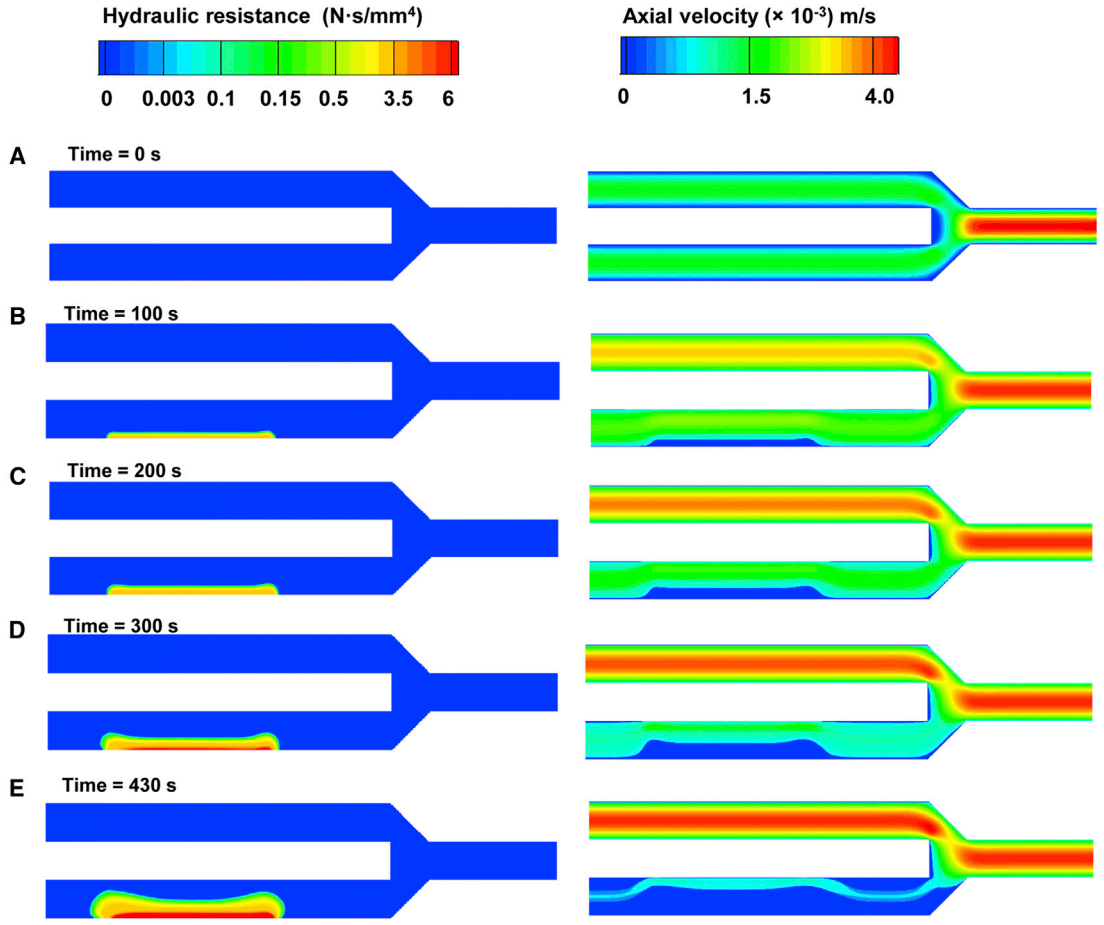

FIGURE 7 Platelet and fibrin deposition occludes the flow through the bottom channel of the flow chamber. (*A–E*) The colors represent the hydraulic resistance (*left*) and axial flow velocity (*right*) in the flow chamber at distinct times in the simulation. To see this figure in color, go online.

appear to complement our findings, because they pertain to the case of fibrinogen deficiency, whereas we consider the case of fibrinogen supplementation (i.e., $\geq$100% fibrinogen). Taken together, these findings may suggest a saturation effect: severely decreased fibrinogen levels may result in a reduction in thrombus size, whereas a moderate increase in the fibrinogen level beyond the typical normal value may only marginally impact thrombus formation and the resulting blood-flow pattern.

We investigated the effect of fibrinogen supplementation on blood flow within the thrombus by analyzing the dependence of the flow's axial velocity on the vertical distance (indicated by the white line in Fig. 8 *C* where fibrin concentration was higher) from the thrombogenic surface. For all considered fibrinogen levels, this dependency had a similar sigmoidal shape (Fig. 8 *D*). As expected, at all distances from the thrombogenic surface, axial flow velocity monotonically decreased upon fibrinogen supplementation. The fibrinogen-dependent decrease in the flow velocity was distance dependent, achieving up to ~1.3-fold magnitude (at 8 μm from the thrombogenic surface). Thus, fibrinogen supplementation can significantly affect blood flow through the fibrin-rich lower portion of the thrombus. Notably, for all considered fibrinogen levels, the axial velocity dependence on the distance from the thrombogenic surface converged to the same plateau for larger distance values (>13 μm from the thrombogenic surface) (Fig. 8 *D*). This result suggests that the effect of fibrinogen supplementation on the blood-flow velocity did not extend beyond a certain height, which was nearly the same for all the fibrinogen supplementation levels. That height can be interpreted as the boundary of the thrombus-occupied area where relatively less fibrin was present, but which was rich in platelets. This is consistent with our finding that the shape and size of the area of reduced axial velocity (i.e., the outer shape and size of the thrombus) was generally determined by the area of platelet deposition, which extended beyond the area of fibrin deposition.

Fibrinogen and PCC supplementation increase the thrombus hydraulic resistance during blood dilution

In our simulations, as expected (63), the level of generated thrombin was strongly reduced (by ~3.1-fold) by dilution

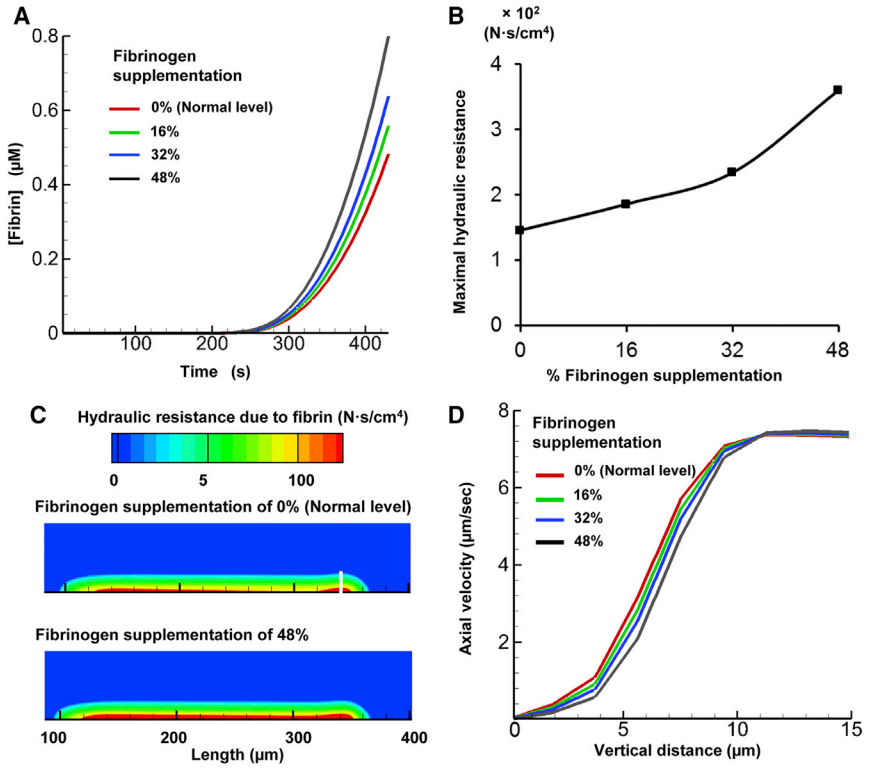

FIGURE 8 The model predicted an increase in hydraulic resistance upon fibrinogen supplementation. (*A*) Fibrin generation for various fibrinogen supplementation levels (16%, 32%, and 48% beyond the normal level of 5.4 μM). (*B*) Maximal hydraulic resistance imparted by the generated fibrin in the flow chamber at 430 s. The initial data point (at 0% supplemented fibrinogen level) represents the maximal resistance imparted at the default fibrinogen level. (*C*) Spatial distribution of hydraulic resistance imparted by normal fibrinogen level and by 48% fibrinogen supplementation at 430 s. (*D*) Flow axial velocity plotted against the vertical distance from the thrombogenic surface at the region of maximal hydraulic resistance (indicated by the *white line* in C) within the clot at 430 s. Each axial velocity curve corresponds to one of the considered fibrinogen levels. To see this figure in color, go online.

and unaffected by fibrinogen supplementation (Fig. 9 *A*). Interestingly, an in vitro experimental study conducted by Bolliger et al. reported that thrombin is reduced by ~2.3-fold under plasma dilution (71). In our model simulations, the fibrin level was also significantly reduced by dilution (at 430 s, by at least an order of magnitude), and fibrinogen supplementation had a strongly nonlinear effect on fibrin generation (Fig. 9 *B*). Indeed, at 430 s, the fibrin level for 16% supplemented fibrinogen was ~1.5-fold higher than that in unsupplemented blood, but only marginally lower than in the cases of 32% and 48% supplemented fibrinogen. Moreover, in the latter case, the total fibrinogen level was 88% of its normal undiluted value, but the corresponding level of fibrin at 430 s was ~5-fold lower than normal (Fig. 9 *B*). This could be attributed to the fact that the rate of fibrin production is proportional to the product of the thrombin and fibrinogen concentrations (Eq. S29), and the dilution-reduced thrombin concentration did not increase under fibrinogen supplementation. This is consistent with the conclusion made by Bolliger et al. that fibrinogen supplementation by ~100% of the normal value is required for optimized clot formation (71). Our results on fibrinogen supplementation in diluted blood are also consistent with our previously obtained simulation results showing that fibrinogen supplementation alone does not fully restore the normal fibrin kinetics (72). At the same time, additional supplementation with a PCC increased thrombin concentration by ~2.75-fold, thus producing a thrombin level that was ~85% of its normal value (Fig. 9 *A*). This extra thrombin increased the generated fibrin level, which at 430 s was ~80% of its normal value (Fig. 9 *B*).

To assess the functional consequences of dilution/supplementation-induced differences in the fibrin level, we compared the hydraulic resistance inside the thrombus for unsupplemented diluted blood with that for fibrinogen-supplemented and PCC+fibrinogen-supplemented diluted blood. The increase in fibrin generation due to PCC+fibrinogen supplementation increased the hydraulic resistance by ~8-fold (Fig. 9 *C*). Furthermore, we analyzed the axial flow velocity inside the thrombus for diluted and supplemented blood (Fig. 9 *D*). As expected, dilution increased the flow velocity, reflecting a relatively weaker ability of the clot to resist blood flow. The dependence of the axial velocity on the amount of supplemented fibrinogen was strongly nonlinear. The blood-flow velocity in the thrombus region for all fibrinogen supplementation levels was considerably lower than that in unsupplemented diluted blood. Although this implies that fibrinogen supplementation can improve hemostasis (Fig. 9 *D*), even the 48% fibrinogen supplementation could not (approximately) restore the normal (i.e., predilution) flow-velocity value. At the same time, PCC and 48% fibrinogen supplementation nearly restored the interthrombus blood velocity to its normal value (Fig. 9 *D*). Taken together, our results suggest that under blood dilution conditions, normal clot formation cannot be restored by fibrinogen supplementation alone, and simultaneous enhancement of thrombin generation is preferable. This can be achieved using additional clotting-factor

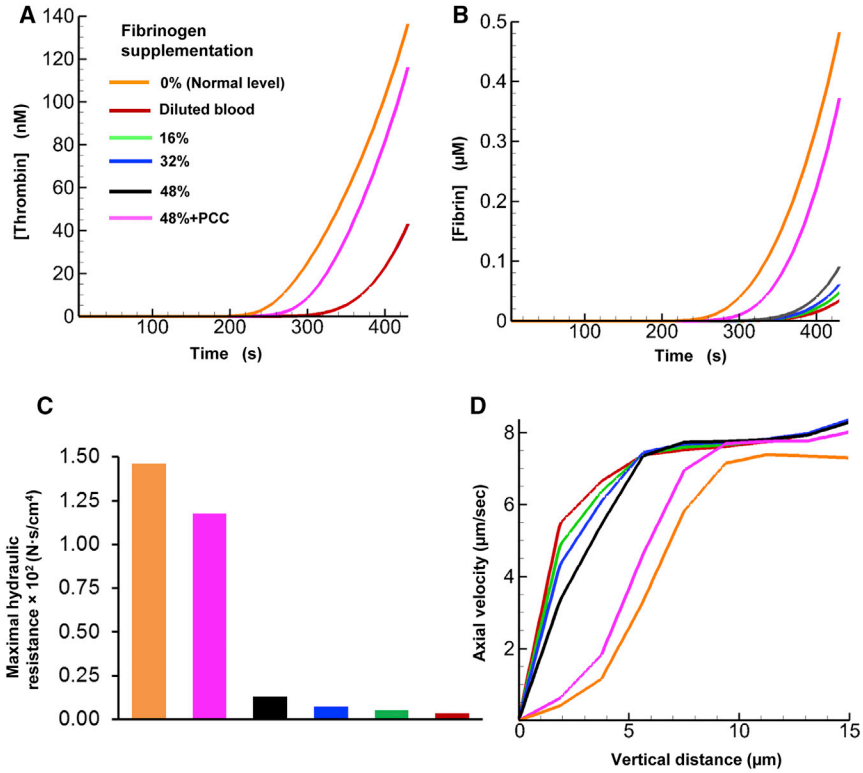

FIGURE 9 Effects of blood dilution, fibrinogen supplementation, and PCC supplementation on thrombus development. (*A*) Thrombin generation for various fibrinogen supplementation levels (16%, 32%, and 48% of 5.4 μM beyond the diluted level of 2.16 μM and PCC supplementation). Note that the thrombin level did not change during fibrinogen supplementation hence the overlap between the curves for diluted blood and those for fibrinogen supplementation. (*B*) Fibrin generation for various fibrinogen supplementation levels and 48%+PCC fibrin supplementation. (*C*) Maximal hydraulic resistance imparted by generated fibrin for different fibrinogen supplementation levels and for 48%+PCC fibrin supplementation at 430 s. (*D*) Flow axial velocity plotted against the vertical distance from the thrombogenic surface at the region of maximal hydraulic resistance within the clot at 430 s. Each axial velocity curve corresponds to one of the considered fibrinogen supplementation levels. To see this figure in color, go online.

supplements, such as a PCC. This conclusion is consistent with our previously obtained in vitro blood coagulation simulation results and implies that fibrinogen should be used in combination with other clotting factors to improve clot formation in coagulopathy (65,72).

DISCUSSION

Normal functioning of the blood coagulation system is essential for human survival, which continues to motivate attempts to clarify the mechanistic details of blood clotting. Despite extensive research, the time-dependent spatial organization, and its connection with the functional properties, of a growing thrombus have not been fully understood. Yet such understanding may be critical for our ability to predict and control thrombus growth, including its modulation by therapeutic interventions. Here, we developed a computational model of thrombus formation in a flow chamber (Figs. 3 and 4) based on the framework previously developed by Leiderman and Fogelson (22). We extended that framework by 1) including explicit representations of fibrin generation; 2) implementing an enhanced platelet and biochemical species diffusivity model with a varying hematocrit profile; 3) implementing a field potential function in the mobile-platelets-governing equation to account for platelet margination due to the presence of red blood cells; 4) implementing a shear-dependent platelet-adhesion rate constant to represent the effect of shear rate on platelet adhesion; 5) adding specific binding sites for zymogens and enzymes on platelet surfaces, with binding-site numbers obtained from the literature and factor X sharing the binding sites with prothrombin; 6) implementing the activation of prothrombin to thrombin in plasma by the action of factor Xa; and 7) reflecting the contributions of fibrin to the mechanical properties of the growing thrombus. We applied the model to investigate the accumulation of the thrombus' main enzymatic component (i.e., thrombin) and structural components (i.e., platelets and fibrin). Our model predicted distinct spatial distribution patterns for platelets, thrombin, and fibrin (Figs. 5 and 6) and identified platelet accumulation as the primary driver of blood-flow occlusion by a growing thrombus (Figs. 5 and 7). Moreover, we used the model to establish the nonlinear dependencies of thrombus characteristics on the amount of supplemented fibrinogen (Fig. 8) and to investigate the effect of fibrinogen and PCC supplementation on thrombus formation in diluted blood (Fig. 9), which has been shown to potentially improve hemostasis in trauma patients with severe bleeding (73,74).

Our model semiquantitatively reproduced the dynamics of platelet deposition and the area of platelet deposition measured in experiments. Similarly to the thrombin dynamics predicted by our model, rapid thrombin accumulation after an initial delay is a salient feature of thrombin generation assays performed in vitro in the absence of flow (i.e., "static" assays) (8,36,75). Likewise, typical kinetic curves of fibrin accumulation in static assays are characterized by a delay followed by a rapid onset of fibrin

generation (8,72). Thrombin generation delay corresponds to its initiation phase, which is due to well-studied thrombin generation biochemistry (36). The time when the thrombin concentration reaches 2–10 nM is known as clotting time and defines the time of onset of fibrin generation (36,75). Thus, delays followed by rapid bursts in thrombin and fibrin accumulation are determined by the basic biochemistry of these processes and therefore should generally be expected. In accord with this expectation, the original LF computational model, applied to thrombus formation in a flow chamber, predicted a pronounced delay followed by a rapid increase in the thrombin concentration (32). Our predictions for thrombin and fibrin generation are consistent with this behavior, as are the flow-chamber measurements by Onasoga-Jarvis et al. (Fig. 4 *B*). The somewhat unexpected early accumulation of fibrin in the flow chamber used by Colace et al. (Fig. 4 *B*) suggests some portions of thrombin, present early, as a possible cause. We performed supplemental simulations with an added amount of thrombin specified at the inlet (all other simulation conditions remained unchanged; see Materials and Methods). The simulations showed that the presence of thrombin in plasma (which may result from accidental activation of the coagulation system during blood sample collection) could indeed result in fibrin accumulation kinetics similar to that observed in the experiment (Fig. S2). Direct thrombin measurements in the experimental system would further clarify the basis for early fibrin accumulation.

The studies of spatial distribution of platelets, thrombin, and fibrin were initiated ~15 years ago in mouse models of blood coagulation using intravital microscopy (1,76). However, due to the differences between mouse and human biochemistry and physiology, such studies provide only partial answers about blood coagulation in the human and should be supplemented by other approaches. Our model of blood coagulation relies on mechanisms and numerical parameter values expected to correspond to the blood coagulation process in humans, and the predicted results can be compared with both flow-chamber experiments and intravital microscopy data.

Consistent with in vivo studies, platelet accumulation and the spreading of fibrin through the thrombus in our simulations occurred as concurrent processes, challenging the traditional paradigm of "platelet plug" formation and fibrin accumulation as distinct processes occurring one after the other (1). Furthermore, in accord with both intravital microscopy data and the flow-chamber experiments of Colace et al. (31), the area of platelet accumulation included and exceeded that of fibrin accumulation. Moreover, consistent with intravital microscopy data, our model predicted the presence of thrombin throughout the thrombus, not just at the thrombus-blood interface (1). Interestingly, the flow-chamber measurements of Colace et al. (31) demonstrate that fibrin accumulates preferentially at the downstream part of the thrombogenic surface and does not extend beyond the platelet accumulation area, which is captured in our modeling predictions for both fibrin and thrombin accumulation. However, intravital microscopy data suggest that fibrin accumulates predominantly at the *upstream* side of the growing platelet thrombus (76), or that the distribution of fibrin is symmetrical about the thrombus center line (77). A plausible reason for these discrepancies is the spatial structure of the experimentally induced lesion that activates thrombus formation in vivo, but the real reason for the discrepancies may lie deeper.

A unique advantage of computational modeling of thrombus formation lies in the possibility of simultaneously predicting both thrombus structure/composition and its physical properties, such as hydraulic resistance and flow velocity inside the thrombus or in its vicinity. Currently used experimental approaches cannot achieve simultaneous measurement of these physical properties. This is why our predictions regarding the correspondence between thrombus structure and blood-flow mechanics cannot be validated by direct comparison with experimental data. However, although it is not preferable, our predictions can be assessed using comparisons with other computational modeling studies. Indeed, computations with the original LF model (which did not represent fibrin accumulation) showed that deposited platelets could effectively slow down and divert the blood flow in their vicinity (22). Interestingly, in that computation, the up- and downstream slopes of the area of reduced flux velocity near the thrombus were more gradual than the slopes of the area of platelet accumulation, which is consistent with our computations. A modeling study that involved a representation of platelets as discrete particles showed that even loose platelet aggregates can noticeably decrease the fluid flow through the area (18). Because the platelet deposition area typically exceeds that of fibrin deposition, these results suggest that the outer boundaries of the thrombus would be defined by the spatial platelet distribution. This pattern was consistently demonstrated in our simulations.

A computational modeling approach offers the possibility of delineating the individual contributions of distinct model features, representing different aspects of the fluid dynamics, chemistry, and biology of blood coagulation. This can be illustrated by a brief comparison of the current version of our model (considered in this article) and earlier model versions. The current version of our model incorporates a number of added features (such as platelet binding sites with protein-specific binding constants, prothrombin activation in plasma, and ADP-dependent platelet activation), some (or all) of which were absent in earlier model versions. For a number of model versions that incorporate different subsets of these features, we analyzed the deposition of platelets and the generation of thrombin and fibrin, as well as the flow axial velocity inside the growing thrombus. We found that the most recent model extensions (namely, the incorporation of initially reversible platelet capture,

the use of a shear-dependent platelet adhesion rate constant, explicit modeling of platelet margination, and the use of local shear rate in Eq. 2) resulted in the following two qualitative changes in model behavior. First, the platelet deposition height profile shows "bumps" on the upstream and downstream sides (Fig. 3 *B*) that were absent in our simulations with earlier model versions. Second, the spatial growth of thrombin and fibrin is characterized by a more evenly distributed profile (Fig. 6), compared to the earlier model versions during the first 430 s of thrombus growth. The presence or absence of other above-mentioned model features did not change the model properties and resulted only in moderate (up to ~30%) quantitative changes in the considered outputs. Yet it is conceivable that the differences caused by the added model features could be larger for other (e.g., arterial) flow conditions and other domains (i.e., flow-chamber or blood-vessel geometries).

Our modeling prediction that the timing of the onset of fibrin generation is insensitive to fibrinogen supplementation, whereas the final fibrin level is not, is in accord with experimental and modeling results for static fibrin generation assays (12,72). The fibrinogen-modulated increase in the amount of deposited fibrin and the resulting increase in hydraulic resistance inside the thrombus were to be expected. However, the interpretation of the clinical data on fibrinogen-dependent improvements in blood clotting (5,10,11) is less straightforward, given that the function of a thrombus to reduce and divert blood flow is due primarily to the deposited platelets rather than to fibrin. The underlying mechanism for the improvements may be the destruction of the outer, fibrin-free layer of the thrombus by the oncoming blood flow, which may slow down the overall speed of thrombus growth. When fibrin generation is stimulated, increased fibrin deposition will stabilize a larger part of the clot; integrated over many clots, this effect may account for the clinical benefits of fibrinogen supplementation.

Our analysis of the blood-flow occlusion due to thrombus formation has implications for the problem of thrombus-size control. Indeed, our computations suggest that, as clot growth proceeds, the flow velocity above the thrombus region increases (due to the conservation of mass for the total blood flow) (Fig. 7). This implies that the increased convective forces will result in more platelets being carried away from the side of the clot facing the lumen. According to our modeling results, the size of the thrombus is determined primarily by platelet deposition. Therefore, platelet "wash-off" is expected to limit the growth rate and the size of the clot. This hypothesis is supported by the computational study of Pivkin et al. (with explicit representation of platelets as individual particles), who observed that thrombus growth rate depends on blood-flow velocity and that after an initial increase in clot size, portions of thrombus can break off and be carried away as emboli (25). In contrast, other computational modeling studies propose alternative mechanisms of clot-size control. One such mechanism is the hindered transport of coagulation proteins into the thrombus in regions of high platelet density, which was suggested in a study based on the use of the LF model (22,69). Moreover, some studies have suggested that fibrin does not have a large impact on protein diffusive transport (78), and others have reported that fibrin decreases the permeability of the thrombus (79). Our analysis suggests that because the local flow velocity in the clot is reduced due to both platelets and fibrin, increased density of either one can slow down the transport of coagulation proteins into the thrombus. In fact, our study shows that fibrin-rich thrombus regions impart a larger hydraulic resistance (inverse of permeability) compared to regions with lower fibrin concentrations (Figs. 6 and 7). This results in a greater reduction of the local flow velocity in fibrin-rich regions of the thrombus (Fig. S3) and thus seems to support the hypothesis that fibrin may alter the flow, and hence the transport, of proteins due to a decreased permeability (79,80).

Another possible mechanism of clot-size control is the formation of a "fibrin cap" on the surface of the thrombus, which impedes thrombin diffusion, thereby restricting the activation of additional platelets and the formation of additional fibrin molecules (81). This is consistent with experimental results from the same group (78). Because our study suggests that the domain of fibrin accumulation does not exceed that of platelet accumulation (which is in accord with computational (70) and experimental (31,82) results by other groups), it does not provide a strong support for the fibrin-cap hypothesis under the considered simulation conditions. A likely contributor to thrombus-size control is the naturally occurring process of fibrinolysis, which may take place on the same timescale as thrombus formation (72). Further computational and experimental studies are warranted to assess the possibility of simultaneous contributions of all these mechanisms to thrombus-size control, as well as to identify predominant mechanisms and their dependence on clot-formation conditions.

The modeling study reported in this article has a number of limitations. First, this is a computational study, and much remains to be done to ensure proper experimental validation of all our computational predictions. Comparisons with experimental data reported here show that the model can reproduce several salient features of clot formation under flow (Figs. 3 and 4). Second, this work represents thrombus formation in a flow chamber, which only partially represents blood coagulation in vivo. Yet flow-chamber experiments provide the control and flexibility that cannot be achieved by other experimental or observational techniques, and they define an important step toward understanding how blood clots in the body. Third, our model gives a simplified representation of the thrombus-formation process. Indeed, our 2D model contains a reduced biochemical model of thrombin generation, does not account for fibrin polymerization or fibrinolysis, and does not explicitly represent platelets and red blood cells as mechanical bodies flowing

with the blood. As a result, our model does not explicitly represent platelet-fibrin interactions and the dependence of platelet-platelet interactions on fibrin levels. Nevertheless, computational-fluid-dynamics-based approaches similar to ours can generate modeling predictions consistent with experimental data and yield insights useful for the understanding of thrombus formation as a kinetic process. This is because they provide a reasonable compromise between the intention to accurately reflect clot formation and the extreme mechanistic complexity of this process (17,20,22,24,26–28,34).

This work investigates thrombus formation as a process developing (primarily) in two dimensions. However, the representation of the physical and chemical processes in the model can be immediately extended to three dimensions and applied to model blood coagulation in realistic blood vessel geometries and flow conditions, including the presence of hemorrhage from a breached vessel. Our work thus defines a direction for future investigations aimed at generating testable hypotheses about thrombus formation in vivo. Furthermore, such an approach can be extended to provide strategies for predictive analysis of the effects of pharmacologic agents on blood clotting in the human body. Improvements in the accuracy of our model's components will allow us to increase and test our understanding of blood coagulation as a natural phenomenon.

SUPPORTING MATERIAL

Model equations, three figures, and nine tables are available at http://www.biophysj.org/biophysj/supplemental/S0006-3495(16)30059-5.

AUTHOR CONTRIBUTIONS

V.G., V.R., J.R., and A.Y.M designed the research. V.G., V.R., and A.Y.M performed the research. V.G., V.R., J.R., and A.Y.M analyzed the data. V.G., J.R., and A.Y.M wrote the article.

ACKNOWLEDGMENTS

The authors are grateful to Drs. Scott Diamond, Karin Leiderman, and Konstantinos Vogiatzis for valuable discussions, and to four anonymous reviewers whose comments and suggestions helped the authors to improve the article. The opinions and assertions contained herein are the private views of the authors and are not to be construed as official or as reflecting the views of the U.S. Army or of the U.S. Department of Defense. This article has been approved for public release with unlimited distribution.

This work was supported by the U.S. Army Network Science Initiative, U.S. Army Medical Research and Materiel Command, Fort Detrick, MD. High-performance computing resources were made available by the U.S. Department of Defense High Performance Computing Modernization Program.

SUPPORTING CITATIONS

References (83–98) appear in the Supporting Material.

REFERENCES

1. Furie, B., and B. C. Furie. 2007. In vivo thrombus formation. *J. Thromb. Haemost.* 5 (*Suppl 1*):12–17.
2. Monroe, D. M., and M. Hoffman. 2006. What does it take to make the perfect clot? *Arterioscler. Thromb. Vasc. Biol.* 26:41–48.
3. Spronk, H. M., J. W. Govers-Riemslag, and H. ten Cate. 2003. The blood coagulation system as a molecular machine. *BioEssays.* 25:1220–1228.
4. Undas, A., and R. A. Ariëns. 2011. Fibrin clot structure and function: a role in the pathophysiology of arterial and venous thromboembolic diseases. *Arterioscler. Thromb. Vasc. Biol.* 31:e88–e99.
5. Levy, J. H., F. Szlam, …, R. M. Sniecienski. 2012. Fibrinogen and hemostasis: a primary hemostatic target for the management of acquired bleeding. *Anesth. Analg.* 114:261–274.
6. Machlus, K. R., M. M. Aleman, and A. S. Wolberg. 2011. Update on venous thromboembolism: risk factors, mechanisms, and treatments. *Arterioscler. Thromb. Vasc. Biol.* 31:476–478.
7. Nesbitt, W. S., E. Westein, …, S. P. Jackson. 2009. A shear gradient-dependent platelet aggregation mechanism drives thrombus formation. *Nat. Med.* 15:665–673.
8. Wolberg, A. S. 2007. Thrombin generation and fibrin clot structure. *Blood Rev.* 21:131–142.
9. Mosesson, M. W. 2005. Fibrinogen and fibrin structure and functions. *J. Thromb. Haemost.* 3:1894–1904.
10. Danés, A. F., L. G. Cuenca, …, J. B. Ronsano. 2008. Efficacy and tolerability of human fibrinogen concentrate administration to patients with acquired fibrinogen deficiency and active or in high-risk severe bleeding. *Vox Sang.* 94:221–226.
11. Karlsson, M., L. Ternström, …, A. Jeppsson. 2009. Prophylactic fibrinogen infusion reduces bleeding after coronary artery bypass surgery. A prospective randomised pilot study. *Thromb. Haemost.* 102:137–144.
12. Machlus, K. R., J. C. Cardenas, …, A. S. Wolberg. 2011. Causal relationship between hyperfibrinogenemia, thrombosis, and resistance to thrombolysis in mice. *Blood.* 117:4953–4963.
13. Brown, A. E., R. I. Litvinov, …, J. W. Weisel. 2009. Multiscale mechanics of fibrin polymer: gel stretching with protein unfolding and loss of water. *Science.* 325:741–744.
14. Ryan, E. A., L. F. Mockros, …, L. Lorand. 1999. Structural origins of fibrin clot rheology. *Biophys. J.* 77:2813–2826.
15. Diamond, S. L. 2013. Systems biology of coagulation. *J. Thromb. Haemost.* 11 (*Suppl 1*):224–232.
16. Xu, Z., M. Kamocka, …, E. D. Rosen. 2011. Computational approaches to studying thrombus development. *Arterioscler. Thromb. Vasc. Biol.* 31:500–505.
17. Anand, M., K. Rajagopal, and K. R. Rajagopal. 2005. A model for the formation and lysis of blood clots. *Pathophysiol. Haemost. Thromb.* 34:109–120.
18. Flamm, M. H., T. V. Colace, …, S. L. Diamond. 2012. Multiscale prediction of patient-specific platelet function under flow. *Blood.* 120:190–198.
19. Fogelson, A. L., and N. Tania. 2005. Coagulation under flow: the influence of flow-mediated transport on the initiation and inhibition of coagulation. *Pathophysiol. Haemost. Thromb.* 34:91–108.
20. Jordan, S. W., and E. L. Chaikof. 2011. Simulated surface-induced thrombin generation in a flow field. *Biophys. J.* 101:276–286.
21. Kuharsky, A. L., and A. L. Fogelson. 2001. Surface-mediated control of blood coagulation: the role of binding site densities and platelet deposition. *Biophys. J.* 80:1050–1074.
22. Leiderman, K., and A. L. Fogelson. 2011. Grow with the flow: a spatial-temporal model of platelet deposition and blood coagulation under flow. *Math. Med. Biol.* 28:47–84.
23. Mori, D., K. Yano, …, T. Yamaguchi. 2008. Simulation of platelet adhesion and aggregation regulated by fibrinogen and von Willebrand factor. *Thromb. Haemost.* 99:108–115.

24. Panteleev, M. A., M. V. Ovanesov, …, F. I. Ataullakhanov. 2006. Spatial propagation and localization of blood coagulation are regulated by intrinsic and protein C pathways, respectively. *Biophys. J.* 90:1489–1500.

25. Pivkin, I. V., P. D. Richardson, and G. Karniadakis. 2006. Blood flow velocity effects and role of activation delay time on growth and form of platelet thrombi. *Proc. Natl. Acad. Sci. USA.* 103:17164–17169.

26. Rugonyi, S., E. Tucker, …, S. Hanson. 2010. Transport-reaction model of mural thrombogenesis: comparisons of mathematical model predictions and results from baboon models. *Ann. Biomed. Eng.* 38:2660–2675.

27. Sorensen, E. N., G. W. Burgreen, …, J. F. Antaki. 1999. Computational simulation of platelet deposition and activation: II. Results for Poiseuille flow over collagen. *Ann. Biomed. Eng.* 27:449–458.

28. Sorensen, E. N., G. W. Burgreen, …, J. F. Antaki. 1999. Computational simulation of platelet deposition and activation: I. Model development and properties. *Ann. Biomed. Eng.* 27:436–448.

29. Tosenberger, A., F. Ataullakhanov, …, V. Volpert. 2013. Modelling of thrombus growth in flow with a DPD-PDE method. *J. Theor. Biol.* 337:30–41.

30. Xu, Z., J. Lioi, …, M. Alber. 2010. A multiscale model of venous thrombus formation with surface-mediated control of blood coagulation cascade. *Biophys. J.* 98:1723–1732.

31. Colace, T. V., R. W. Muthard, and S. L. Diamond. 2012. Thrombus growth and embolism on tissue factor-bearing collagen surfaces under flow: role of thrombin with and without fibrin. *Arterioscler. Thromb. Vasc. Biol.* 32:1466–1476.

32. Onasoga-Jarvis, A. A., K. Leiderman, …, K. B. Neeves. 2013. The effect of factor VIII deficiencies and replacement and bypass therapies on thrombus formation under venous flow conditions in microfluidic and computational models. *PLoS One.* 8:e78732.

33. Onasoga-Jarvis, A. A., T. J. Puls, …, K. B. Neeves. 2014. Thrombin generation and fibrin formation under flow on biomimetic tissue factor-rich surfaces. *J. Thromb. Haemost.* 12:373–382.

34. Neeves, K. B., D. A. Illing, and S. L. Diamond. 2010. Thrombin flux and wall shear rate regulate fibrin fiber deposition state during polymerization under flow. *Biophys. J.* 98:1344–1352.

35. Krishnaswamy, S. 2013. The transition of prothrombin to thrombin. *J. Thromb. Haemost.* 11 (*Suppl 1*):265–276.

36. Hockin, M. F., K. C. Jones, …, K. G. Mann. 2002. A model for the stoichiometric regulation of blood coagulation. *J. Biol. Chem.* 277:18322–18333.

37. Papadopoulos, K. P., M. Gavaises, and C. Atkin. 2014. A simplified mathematical model for thrombin generation. *Med. Eng. Phys.* 36:196–204.

38. Carroll, G. T., P. D. Devereux, …, M. T. Walsh. 2010. Experimental validation of convection-diffusion discretisation scheme employed for computational modelling of biological mass transport. *Biomed. Eng. Online.* 9:34.

39. Wootton, D. M., and D. N. Ku. 1999. Fluid mechanics of vascular systems, diseases, and thrombosis. *Annu. Rev. Biomed. Eng.* 1:299–329.

40. Skotheim, J. M., and T. W. Secomb. 2007. Red blood cells and other nonspherical capsules in shear flow: oscillatory dynamics and the tank-treading-to-tumbling transition. *Phys. Rev. Lett.* 98:078301.

41. Zydney, A. L., and C. K. Colton. 1988. Augmented solute transport in the shear flow of a concentrated suspension. *Physicochem. Hydrodyn.* 10:77–96.

42. Hund, S. J., and J. F. Antaki. 2009. An extended convection diffusion model for red blood cell-enhanced transport of thrombocytes and leukocytes. *Phys. Med. Biol.* 54:6415–6435.

43. Bark, D. L., Jr., and D. N. Ku. 2013. Platelet transport rates and binding kinetics at high shear over a thrombus. *Biophys. J.* 105:502–511.

44. Crowl, L., and A. L. Fogelson. 2011. Analysis of mechanisms for platelet near-wall excess under arterial blood flow conditions. *J. Fluid Mech.* 676:348–375.

45. Eckstein, E. C., and F. Belgacem. 1991. Model of platelet transport in flowing blood with drift and diffusion terms. *Biophys. J.* 60:53–69.

46. Tokarev, A. A., A. A. Butylin, …, F. I. Ataullakhanov. 2011. Finite platelet size could be responsible for platelet margination effect. *Biophys. J.* 101:1835–1843.

47. Buchanan, J. R., Jr., and C. Kleinstreuer. 1998. Simulation of particle-hemodynamics in a partially occluded artery segment with implications to the initiation of microemboli and secondary stenoses. *J. Biomech. Eng.* 120:446–454.

48. Kumar, A., and M. D. Graham. 2012. Mechanism of margination in confined flows of blood and other multicomponent suspensions. *Phys. Rev. Lett.* 109:108102.

49. Kumar, A., R. G. H. Rivera, and M. D. Graham. 2014. Flow-induced segregation in confined multicomponent suspensions: effects of particle size and rigidity. *J. Fluid Mech.* 738:423–462.

50. Starov, V. M., and V. G. Zhdanov. 2001. Effective viscosity and permeability of porous media. *Colloids Surf. A Physicochem. Eng. Asp.* 192:363–375.

51. Issa, R. I., A. D. Gosman, and A. P. Watkins. 1986. The computation of compressible and incompressible recirculating flows by a non-iterative implicit scheme. *J. Comput. Phys.* 62:66–82.

52. ANSYS. 2012. FLUENT Manual for ANSYS Release Version 14.5; ANSYS, Canonsburg, PA.

53. Patankar, S. V. 1980. Numerical Heat Transfer and Fluid Flow: Computational Methods in Mechanics and Thermal Science. CRC Press, New York.

54. Barrett, R., M. Berry, …, H. Van der Vorst. 1994. Templates for the Solution of Linear Systems: Building Blocks for Iterative Methods. SIAM, Philadelphia, PA.

55. Mattern, K. J., and W. M. Deen. 2008. "Mixing rules" for estimating the hydraulic permeability of fiber mixtures. *AIChE J.* 54:32–41.

56. Wufsus, A. R., N. E. Macera, and K. B. Neeves. 2013. The hydraulic permeability of blood clots as a function of fibrin and platelet density. *Biophys. J.* 104:1812–1823.

57. Adolph, R., D. A. Vorp, …, S. C. Watkins. 1997. Cellular content and permeability of intraluminal thrombus in abdominal aortic aneurysm. *J. Vasc. Surg.* 25:916–926.

58. Weisel, J. W. 2004. The mechanical properties of fibrin for basic scientists and clinicians. *Biophys. Chem.* 112:267–276.

59. Davies, C. N. 1950. The separation of airborne dust and particles. *Arh. Hig. Rada.* 1:393–427.

60. Blombäck, B., K. Carlsson, …, N. Åslund. 1989. Native fibrin gel networks observed by 3D microscopy, permeation and turbidity. *Biochim. Biophys. Acta.* 997:96–110.

61. Diamond, S. L., and S. Anand. 1993. Inner clot diffusion and permeation during fibrinolysis. *Biophys. J.* 65:2622–2643.

62. Wootton, D. M., A. S. Popel, and B. R. Alevriadou. 2002. An experimental and theoretical study on the dissolution of mural fibrin clots by tissue-type plasminogen activator. *Biotechnol. Bioeng.* 77:405–419.

63. Mitrophanov, A. Y., F. R. Rosendaal, and J. Reifman. 2012. Computational analysis of intersubject variability and thrombin generation in dilutional coagulopathy. *Transfusion.* 52:2475–2486.

64. Dickneite, G., B. Doerr, and F. Kaspereit. 2008. Characterization of the coagulation deficit in porcine dilutional coagulopathy and substitution with a prothrombin complex concentrate. *Anesth. Analg.* 106:1070–1077.

65. Mitrophanov, A. Y., F. R. Rosendaal, and J. Reifman. 2012. Therapeutic correction of thrombin generation in dilution-induced coagulopathy: computational analysis based on a data set of healthy subjects. *J. Trauma Acute Care Surg.* 73 (2, Suppl 1):S95–S102.

66. Tanaka, K. A., M. Mazzeffi, and M. Durila. 2014. Role of prothrombin complex concentrate in perioperative coagulation therapy. *J. Intensive Care.* 2:60.

67. Maloney, S. F., L. F. Brass, and S. L. Diamond. 2010. P2Y12 or P2Y1 inhibitors reduce platelet deposition in a microfluidic model of

thrombosis while apyrase lacks efficacy under flow conditions. *Integr Biol (Camb).* 2:183–192.

68. Eckstein, E. C., A. W. Tilles, and F. J. Millero, 3rd. 1988. Conditions for the occurrence of large near-wall excesses of small particles during blood flow. *Microvasc. Res.* 36:31–39.
69. Leiderman, K., and A. L. Fogelson. 2013. The influence of hindered transport on the development of platelet thrombi under flow. *Bull. Math. Biol.* 75:1255–1283.
70. Tosenberger, A., N. Bessonov, and V. Volpert. 2015. Influence of fibrinogen deficiency on clot formation in flow by hybrid model. *Math. Model. Nat. Phenom.* 10:36–47.
71. Bolliger, D., F. Szlam, …, K. A. Tanaka. 2009. Finding the optimal concentration range for fibrinogen replacement after severe haemodilution: an in vitro model. *Br. J. Anaesth.* 102:793–799.
72. Mitrophanov, A. Y., A. S. Wolberg, and J. Reifman. 2014. Kinetic model facilitates analysis of fibrin generation and its modulation by clotting factors: implications for hemostasis-enhancing therapies. *Mol. Biosyst.* 10:2347–2357.
73. Schöchl, H., L. Forster, …, W. Voelckel. 2010. Use of rotation thromboelastometry (ROTEM) to achieve successful treatment of polytrauma with fibrinogen concentrate and prothrombin complex concentrate. *Anaesthesia.* 65:199–203.
74. Schöchl, H., U. Nienaber, …, C. Solomon. 2010. Goal-directed coagulation management of major trauma patients using thromboelastometry (ROTEM)-guided administration of fibrinogen concentrate and prothrombin complex concentrate. *Crit. Care.* 14:R55.
75. Mitrophanov, A. Y., and J. Reifman. 2011. Kinetic modeling sheds light on the mode of action of recombinant factor VIIa on thrombin generation. *Thromb. Res.* 128:381–390.
76. Falati, S., P. Gross, …, B. Furie. 2002. Real-time in vivo imaging of platelets, tissue factor and fibrin during arterial thrombus formation in the mouse. *Nat. Med.* 8:1175–1181.
77. Ivanciu, L., S. Krishnaswamy, and R. M. Camire. 2012. Imaging coagulation reactions in vivo. *Thromb. Res.* 129 (*Suppl 2*):S54–S56.
78. Kim, O. V., Z. Xu, …, M. S. Alber. 2013. Fibrin networks regulate protein transport during thrombus development. *PLOS Comput. Biol.* 9:e1003095.
79. Muthard, R. W., and S. L. Diamond. 2012. Blood clots are rapidly assembled hemodynamic sensors: flow arrest triggers intraluminal thrombus contraction. *Arterioscler. Thromb. Vasc. Biol.* 32:2938–2945.
80. Welsh, J. D., T. J. Stalker, …, L. F. Brass. 2014. A systems approach to hemostasis: 1. The interdependence of thrombus architecture and agonist movements in the gaps between platelets. *Blood.* 124:1808–1815.
81. Xu, Z., S. Christley, …, M. Alber. 2012. Multiscale model of fibrin accumulation on the blood clot surface and platelet dynamics. *Methods Cell Biol.* 110:367–388.
82. Stalker, T. J., E. A. Traxler, …, L. F. Brass. 2013. Hierarchical organization in the hemostatic response and its relationship to the platelet-signaling network. *Blood.* 121:1875–1885.
83. Tokarev, A. A., A. A. Butylin, and F. I. Ataullakhanov. 2011. Platelet adhesion from shear blood flow is controlled by near-wall rebounding collisions with erythrocytes. *Biophys. J.* 100:799–808.
84. Reed, G. L., M. L. Fitzgerald, and J. Polgár. 2000. Molecular mechanisms of platelet exocytosis: insights into the "secrete" life of thrombocytes. *Blood.* 96:3334–3342.
85. Lages, B. 1986. In vitro platelet responses: dense granule secretion. *In* Platelet Responses and Metabolism Vol. I: Responses. H. Holmsen, editor. CRC Press, Boca Raton, FL.
86. Zhang, J., P. C. Johnson, and A. S. Popel. 2008. Red blood cell aggregation and dissociation in shear flows simulated by lattice Boltzmann method. *J. Biomech.* 41:47–55.
87. Jafari, A., S. M. Mousavi, and P. Kolari. 2008. Numerical investigation of blood flow. Part I: In microvessel bifurcations. *Commun. Nonlinear Sci. Numer. Simul.* 13:1615–1626.
88. Papaioannou, T. G., and C. Stefanadis. 2005. Vascular wall shear stress: basic principles and methods. *Hellenic J. Cardiol.* 46:9–15.
89. Mann, K. G., M. E. Nesheim, …, S. Krishnaswamy. 1990. Surface-dependent reactions of the vitamin K-dependent enzyme complexes. *Blood.* 76:1–16.
90. Mann, K. G., E. G. Bovill, and S. Krishnaswamy. 1991. Surface-dependent reactions in the propagation phase of blood coagulation. *Ann. N. Y. Acad. Sci.* 614:63–75.
91. Morrissey, J. H. 1995. Tissue factor modulation of factor VIIa activity: use in measuring trace levels of factor VIIa in plasma. *Thromb. Haemost.* 74:185–188.
92. Novotny, W. F., S. G. Brown, …, G. J. Broze, Jr. 1991. Plasma antigen levels of the lipoprotein-associated coagulation inhibitor in patient samples. *Blood.* 78:387–393.
93. Scandura, J. M., S. S. Ahmad, and P. N. Walsh. 1996. A binding site expressed on the surface of activated human platelets is shared by factor X and prothrombin. *Biochemistry.* 35:8890–8902.
94. Brass, L. F., M. Ahuja, …, J. A. Hoxie. 1994. The human platelet thrombin receptor. Turning it on and turning it off. *Ann. N. Y. Acad. Sci.* 714:1–12.
95. Walsh, P. N., and A. H. Schmaier. 1994. Platelet-coagulant protein interactions. *In* Hemostasis and Thrombosis: Basic Principles and Clinical Practice, 3rd ed. R. W. Colman, J. Hirsh, V. J. Marder, and E. W. Salzman, editors. Lippincott, Philadelphia, PA, pp. 629–651.
96. Ahmad, S. S., J. M. Scandura, and P. N. Walsh. 2000. Structural and functional characterization of platelet receptor-mediated factor VIII binding. *J. Biol. Chem.* 275:13071–13081.
97. Ahmad, S. S., R. Rawala-Sheikh, and P. N. Walsh. 1989. Comparative interactions of factor IX and factor IXa with human platelets. *J. Biol. Chem.* 264:3244–3251.
98. Mann, K. G., S. Krishnaswamy, and J. H. Lawson. 1992. Surface-dependent hemostasis. *Semin. Hematol.* 29:213–226.